

Publication Title: Bi-directional Charging in V2G Systems: An In-Cell Variation Analysis of Vehicle Batteries

Authors: Haris M. Khalid and Jimmy C.-H. Peng

Disclaimer: This is the authors' version of an article published in early access of IEEE Systems Journal. Changes were made to this version by the publisher prior to publication.

DOI: [10.1109/JSYST.2019.2958967](https://doi.org/10.1109/JSYST.2019.2958967)

Bi-directional Charging in V2G Systems: An In-Cell Variation Analysis of Vehicle Batteries

Haris M. Khalid, *Member, IEEE*, and Jimmy C.-H. Peng, *Member, IEEE*

Abstract—Vehicle-to-Grid (V2G) technology enables bi-directional charging of electric vehicle (EV) and facilitates power grid ancillary services. However, battery pack in EV may develop in-cell dynamic variations over time. This is due to the structural complexity and electrochemical operations in the battery pack. These variations may arise in V2G systems due to 1) additional charging and discharging cycles to power grid, 2) external shocks, and 3) long exposures to high temperatures. A particular source of these variations are due to faulty sensors. Therefore, it can be argued that the battery packs in EV are highly reliant on the monitoring of these in-cell variations and their impact of propagation with each involved component. In this paper, a prediction-based scheme to monitor health of variation induced sensors is proposed. Firstly, a propagation model is developed to predict the in-cell variations of a battery pack by calculating the covariance using a median-based expectation. Secondly, a hypothesis model is developed to detect and isolate each variation. This is obtained by deriving a conditional probability-based density function for the measurements. The proposed monitoring framework is evaluated using experimental measurements collected from Li-ion battery pack in electric vehicles. The in-cell variation profiles have been verified using D-SAT Chroma 8000ATS hardware platform. The performance results of the proposed scheme shows accurate analysis of these emerged variations.

Index Terms—battery degradation, battery pack voltage, bi-directional charging, cell-to-cell variations, electric vehicles, estimation, expected value, grid-to-vehicle, hypothesis testing, in-cell, Li-ion batteries, median filter, prediction, recursive, smart grid, variation propagation, vehicle-to-grid.

I. INTRODUCTION

VEHICULAR technologies such as V2G and G2V can smooth the generation ripples of intermittent renewable energy in the electric power grids [1–5]. In particular, the battery packs in electric vehicles (EVs) can be utilized to participate in ancillary services such as demand response (DR) program [6–8]. This owes to the high energy density provided by the mainstream Li-ion batteries, which are facilitated by efficient grid-connected chargers [9, 10]. However, Li-ion battery packs have a complicated structure, and comprises of hundreds of cells. These cells are connected in a circuit combination of series or parallel. The structure becomes more complicated when these arrays of cells-based batteries are equipped with numerous parametric indicators like power capacity, voltage, current, temperature, etc. As a result, the battery pack of an EV is a very sensitive entity as small variations can affect their complicated hierarchy. For instance, the temperature variation serves as an alarming indicator. A rise in temperature due to the frequent charging and discharging may rupture the battery electrolytes, resulting in their decomposition and production of combustible gases. This may also cause fire and thermal runaway [11, 12]. Similarly, a sudden drop in temperature may cause a failure and malfunction of the cathode, leading

H. M. Khalid is with the Department of Electrical and Electronics Engineering, Higher Colleges of Technology (HCT), Sharjah 7947, UAE, (e-mail: harism.khalid@yahoo.com, webpage: www.harismkhalid.com)

J. C.-H. Peng is with the Department of Electrical and Computer Engineering, National University of Singapore, Singapore, (e-mail: jpeng@nus.edu.sg, webpage: www.penglaboratory.com)

ACRONYMS AND ABBREVIATIONS OF MATHEMATICAL FORMULATIONS

BMS	Battery Management System
DR	Demand Response
EKF	Extended Kalman filter
EV	Electric Vehicle
KF	Kalman filter
G2V	Grid-to-Vehicle
Li-ion	Lithium ion
MSE	Mean Square Error
PAR	peak-to-average ratio
SoC	State-of-Charge
SoH	State-of-Health
UKF	Unscented Kalman filter
V2G	Vehicle-to-Grid
$E_{\mu_{1/2}}$	median expectation operator
$c1$	cell 1
$c2$	cell 2
C	fused form of cells
N	number of in-series connections
I	state of current
F	modal matrix
α	transition matrix of temperature
T	temperature
var	dynamic variations
β	transition matrices of impedance
z	impedance
z_0	standard value of impedance
G	transition matrices of noise
w	random process noise
t	time-instant
y	observations output
H	observation matrix
v	observation noise
T	number of time-instants
p	number of simultaneous observations
V_1	input voltage
V_2	output voltage
P	covariance matrix
ω	weight
δ	difference between individual current estimates
CR	correlated component
UC	uncorrelated component
γ	innovation
Δ	perturbation
θ	gradient
ψ	data-vector
M	hypothesis model
S	variance
$g(\cdot)$	conditional probability density function
j	number of corrupted cells
D	Mahalanobis distance
m	elements in measurement vector

to a short-circuit [11, 13, 14]. This may also result in an imprecise calculation of State-of-Charge (SoC), thus amplifying the problems by triggering the overcharge or discharge mechanism [15, 16]. Therefore, an effective Battery Management System (BMS) is required to protect Li-ion battery packs from these issues [17–19]. BMS has also been used to provide diagnostic and prognostic functions at the component-level [18, 19], and at the system-level [20].

Among the published work, data given by sensors to the BMS

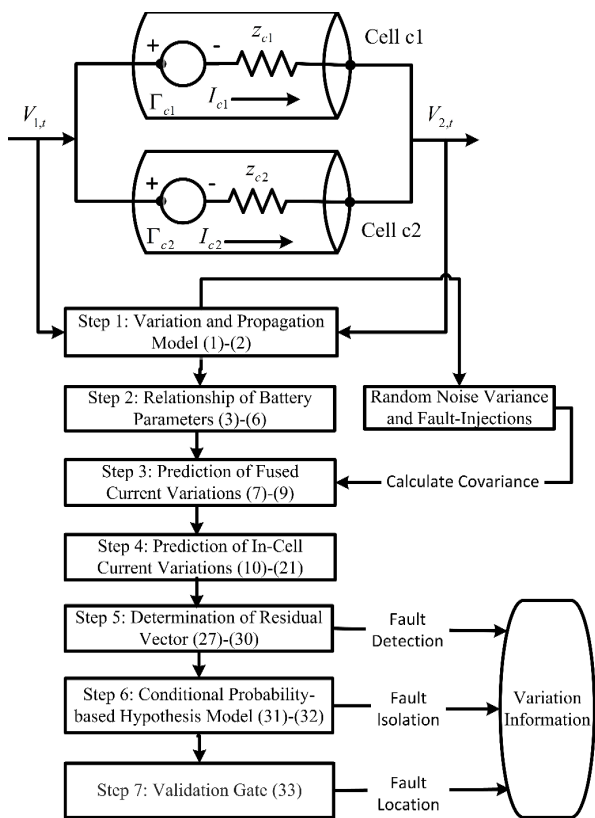


Fig. 2. Seven step-based formulation framework of the proposed scheme

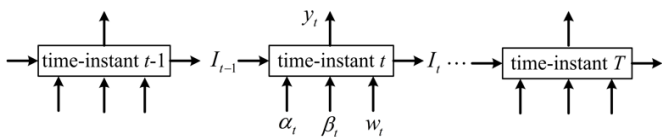


Fig. 3. Variation and propagation in a time-variant process

I_0, I_1, \dots, I_T).

II. PROPOSED SCHEME

The proposed scheme comprises of a formulation framework which involves seven steps.

A. Seven-Step Based Formulation Framework

The seven-step based formulation framework is illustrated in Fig. 2. It summarizes the formulation and equations involved at each step as follows: 1) The proposed methodology begins with developing an in-cell variation propagation model. The assumed system model considered an array of parallel cells connected in a string of series. 2) A relationship between battery parameters in a battery pack is developed. The prediction-based estimation methodology is then built on it for calculating both the 3) fused, and the 4) in-cell current variations respectively. The diagnosis of vehicle battery pack is made by 5) extracting the residual vector, 6) conditional probability-based hypothesis testing, and 7) validation gate.

Note that a standard Li-ion vehicle battery-pack structure of

two parallel cells connected in a thread of N number of series is considered [29]. In this structure, the in-cell variations are dependent on the split of current between two parallel cells. Thus, the variation model is built on the state current I_t .

1) *Step 1 - Variation and Propagation Model:* Consider a discrete-time dynamical model of a vehicle battery-pack involving cells $c1$ and $c2$. These cells are connected in parallel with a voltage supply to N number of in-series connections at time-instant t . The cell dynamics always have variations in a time-variant process. This can be further expressed in Fig. 3. At time-instant t , the cell dynamics are represented by state of current I_t , and the observations output y_t . As it is a time-variant process, the cell-dynamics will show variations at each instant. The main variation inputs consist of α_t , β_t and G_t , which present the transition matrices of temperature, impedance and noise respectively. I_t is related to the deviation of measurements in y_t with F_t and H_t , which represents the modal matrix and mapping observation matrix respectively. T refers to the number of time-instants. A state difference equation can be further described in the deviation propagation as:

$$I_{t+1}^C = F_t^C I_t^C + \frac{\alpha_t^C}{2} (\Gamma_t^{c1} + \Gamma_t^{c2}) I_t^{var} + \beta_t^C (z_t^{c1} + z_t^{c2}) I_t^{var} + G_t^C w_t^C \quad (1)$$

$$y_t^C = H_t^C F_t^C I_t^C + \nu_t^C \quad (2)$$

where the superscript $c1$ represents cell 1, and superscript $c2$ denotes cell 2. The symbol C is used to present the fused form of cells $c1$ and $c2$, i.e. $C = c1 + c2$, whereas C' presents the transpose of this fused form. The symbol var presents the dynamic variations in cells. The $I_0^C \in \mathbf{R}^r$ represents an initial condition of the current state, $F_t^C \in \mathbf{R}^{r \times r}$ is a modal matrix of the state response of current, such that it depends on covariates, $\alpha_t^C \in \mathbf{R}^{r \times r}$ is the transition matrix of temperatures $\Gamma_t^{c1} \in \mathbf{R}^r$ and $\Gamma_t^{c2} \in \mathbf{R}^r$ of cells $c1$ and $c2$ respectively. Also, $\beta_t^C \in \mathbf{R}^{r \times r}$ is the impedance transition matrix of impedances $z_t^{c1} \in \mathbf{R}^r$ and $z_t^{c2} \in \mathbf{R}^r$ respectively. $G_t^C \in \mathbf{R}^{r \times r}$ is the noise transition matrix, which can be defined as a probability vector, whose elements are non-negative real numbers and sum to 1. $w_t^C \in \mathbf{R}^r$ is the random process noise. In the observation model (2), $y_t^C \in \mathbf{R}^p$ is the observation output of state of current, p is the number of simultaneous observations for estimation made at time-instant t , $H_t^C \in \mathbf{R}^{p \times r}$ is the observation matrix of current state, I_t^C is the current state matrix, and $\nu_t^C \in \mathbf{R}^p$ is the observation noise. Note the noises w_t and ν_t have been assumed initially uncorrelated zero-median white Gaussian¹.

2) *Step 2 - Relationship between Battery Parameters:* Once the observation model is extracted, the battery parameters and their interrelations collected from sensors are formulated. Note the battery cells are considered here as conducting bodies only. The known parameters of floor of parallel cells connected in a series string are: 1) string voltages, 2) string temperature, and 3) string current.

At time-instant t , current of individual cells $c1$ and $c2$ can be represented as the difference between input voltage $V_{1,t}^C$ and output voltage $V_{2,t}^C$, with respect to the individual cell

¹ White Gaussian is used as an additive to represent a basic noise model. It is represented as Gaussian to portray the effect of random processes. To cover the domain of all possible random processes, it has a normal distribution and uniform power frequency (white) [30]. The median time-domain value for such a distribution is considered here to be zero.

impedance, respectively as:

$$I_t^{c1} = \frac{V_{1,t}^C - V_{2,t}^C}{z_t^{c1}}, I_t^{c2} = \frac{V_{1,t}^C - V_{2,t}^C}{z_t^{c2}} \quad (3)$$

where I_t^{c1} and I_t^{c2} are the individual readings from the current sensor at cells $c1$ and $c2$ respectively. Also, impedances z_t^{c1} and z_t^{c2} for cells $c1$ and $c2$ are:

$$z_t^{c1} = z_t^{c1^0} + \left[1 + \alpha_t^C (\Gamma_t^{c1} - \Gamma_t^{c1^0})\right], \quad (4)$$

$$z_t^{c2} = z_t^{c2^0} + \left[1 + \alpha_t^C (\Gamma_t^{c2} - \Gamma_t^{c2^0})\right] \quad (5)$$

where $z_t^{c1^0}$ and $z_t^{c2^0}$ are the standard values of impedance at room temperature $\Gamma_t^{c1^0}$ and $\Gamma_t^{c2^0}$ respectively. α_t^C is the transition matrix of temperature at cells $c1$ and $c2$.

Note Γ_t^C is assumed here as an average value of temperature for cells $c1$ and $c2$. Thus, the general relation between battery parameters can be expressed as:

$$I_t^C = \frac{z_t^{c1}}{2\alpha_t^C z_t^{c1^0}} + \frac{z_t^{c2}}{2\alpha_t^C z_t^{c2^0}} + \frac{\Gamma_t^{c1^0}}{2} + \frac{\Gamma_t^{c2^0}}{2} - \frac{1}{\alpha_t^C} \quad (6)$$

Once the dynamic relationships between the parameters of the vehicle battery are determined, variation and propagation model is further derived to calculate the covariance matrix. This is a challenging task due to 1) the absence of a battery model, where accuracy of the variation estimation is dependent on the parameters of interaction between cells, and 2) considering the median-based expectation over the classic weighted average to calculate the noisy observations and prior measurements.

3) *Step 3 - Prediction of Fused Current Variations:* Based on the formulated propagation and observation models, the fused current prediction can be derived by the covariance between the cells $c1$ and $c2$. This required some additional properties of median expectation from [20].

Assume $\hat{I}_{t|t}^C$ as the estimated state at time-instant t for the time-sequence T . Given the observation model of (2) and time-sequence $T - 1$, the state prediction of current can be defined. This definition is linearly expressed with a conditional probability as:

$$\begin{aligned} \hat{I}_{t|t-1}^C &= \mathbf{E}_{\mu_{1/2}}[I_t^C | y_{T-1}^C] + \mathbf{E}_{\mu_{1/2}}[I_t^{var} | I_t^C] \\ &= F_t^C \arg \min_{I_t^C} [I_{t-1}^C - \mu_{1/2,t-1}] + \left(\frac{\alpha_t^C}{2} (\Gamma_t^{c1} + \Gamma_t^{c2})\right. \\ &\quad \left.+ \beta_t^C (z_t^{c1} + z_t^{c2})\right) \arg \min_{I_t^{var}} [I_{t-1}^{var} - \mu_{1/2,t-1}] \end{aligned} \quad (7)$$

Taking the difference between (1) and (7) gives:

$$\begin{aligned} &I_t^C - \hat{I}_{t|t-1}^C \\ &= F_t^C I_t^C + \frac{\alpha_t^C}{2} (\Gamma_t^{c1} + \Gamma_t^{c2}) I_t^{var} + \beta_t^C (z_t^{c1} + z_t^{c2}) I_t^{var} + G_t^C w_t^C \\ &\quad - F_t^C \arg \min_{I_t^C} [I_{t-1}^C - \mu_{1/2,t-1}] \\ &\quad - \frac{\alpha_t^C}{2} (\Gamma_t^{c1} + \Gamma_t^{c2}) \arg \min_{I_t^{var}} [I_{t-1}^{var} - \mu_{1/2,t-1}] \\ &\quad - \beta_t^C (z_t^{c1} + z_t^{c2}) \arg \min_{I_t^{var}} [I_{t-1}^{var} - \mu_{1/2,t-1}] \\ &= F_t^C (I_{t-1}^C - \arg \min_{I_t^C} [I_{t-1}^C - \mu_{1/2,t-1}]) + G_t^C w_t^C \\ &\quad + \frac{\alpha_t^C}{2} (\Gamma_t^{c1} + \Gamma_t^{c2}) (I_t^{var} - \arg \min_{I_t^{var}} [I_{t-1}^{var} - \mu_{1/2,t-1}]) \\ &\quad + \beta_t^C (z_t^{c1} + z_t^{c2}) (I_t^{var} - \arg \min_{I_t^{var}} [I_{t-1}^{var} - \mu_{1/2,t-1}]) \end{aligned} \quad (8)$$

Here $I_t^C - \hat{I}_{t|t-1}^C = P_{I,t|t-1}^C$, where $P_{I,t|t-1}^C$ represents the covariance matrix. Taking the median-based expected value for (8) gives:

$$\begin{aligned} P_{I,t|t-1}^C &= F_t^C P_{\mu_{1/2,t-1|t-1}}^C F_t^{C'} + \frac{\alpha_t^C}{2} P_{\mu_{1/2,t-1|t-1}}^{var,\Gamma} \frac{\alpha_t^C}{2} \\ &\quad + \beta_t^C P_{\mu_{1/2,t-1|t-1}}^{var,z} \beta_t^{C'} + G_t^C Q_t^C G_t^{C'} \end{aligned} \quad (9)$$

The estimated state \hat{I}_t^C and the covariance matrix $P_{I,t}^C$ represent the measurement updated equations, which were derived from the first principles based on (7) to (9). However, $P_{I,t}^C$ assumes that both cells have the same dynamics, i.e. the same 1) impedance, 2) operating temperature, and 3) other cell dynamics. This motivates to consider the problem for vehicle battery pack with dynamic in-cell variations.

4) *Step 4 - Prediction of in-Cell Current Variations:* The in-cell variations narrate the dynamics of the individual cells. These are primarily due to the factors, such as: 1) total capacity of cell, 2) internal resistance of cell, and 3) the initial value of SoC, which gives an adequate reason to derive a covariance matrix. This covariance matrix can further represent the dynamical situation of in-cell current estimation. Let $P_{I,t|t}^{c1}$ be the conservative covariance estimate of cell $c1$, such that $P_{I,t|t}^{c1} \geq \mathbf{E}_{\mu_{1/2}}[(\mu_{1/2,t|t}^{c1} - \mathbf{E}_{\mu_{1/2,t|t}}(\mu_{1/2,t|t}^{c1}))(\mu_{1/2,t|t}^{c1} - \mathbf{E}_{\mu_{1/2,t|t}}(\mu_{1/2,t|t}^{c1}))']$, where $\mu_{1/2,t|t}^{c1}$ is the median vector for current at cell $c1$. Note to achieve convergence, the estimated covariance of cell $c1$, $P_{I,t|t}^{c1}$ follows a behavior as: 1) to always calculate an over-estimate of the median-based expected squared difference between the true median of the unknown distribution function of cell $c1$, $\mu_{1/2}^{c1}$, and its estimate $\arg \min[I_{t-1}^{c1} - \mu_{1/2,t-1}^{c1}]$, 2) to assign a weight ω to calculate the split of in-cell current variations among the parallel connection, 3) this weight is then computed in order to determine the trace of split of current, thereby assigning an estimate value to the individual current estimates $\hat{I}_{t|t}^{c1}$ and $\hat{I}_{t|t}^{c2}$ respectively.

$$\begin{aligned} \hat{I}_{t|t}^C &= P_{I,t|t}^C \left(\omega P_{I,t|t}^{c1^{-1}} (F_t^C \hat{I}_{t|t}^{c1} \frac{\alpha_t^C}{2} \Gamma_t^{c1} \beta_t^C z_t^{c1}) \right. \\ &\quad \left. + (1 - \omega) P_{I,t|t}^{c2^{-1}} (F_t^C \hat{I}_{t|t}^{c2} \frac{\alpha_t^C}{2} \Gamma_t^{c2} \beta_t^C z_t^{c2}) \right) \end{aligned} \quad (10)$$

where the difference between $\hat{I}_{t|t}^{c1}$ and $\hat{I}_{t|t}^{c2}$ can be expressed by δ_t^C as follows:

$$\delta_t^C = \hat{I}_{t|t}^{c1} - \hat{I}_{t|t}^{c2} \quad (11)$$

The expression (11) can be normalized further. This is done by using median-based expectation operator as:

$$\begin{aligned} \mathbf{E}_{\mu_{1/2}}[\delta_t^C \delta_t^{C'}] &= \mathbf{E}_{\mu_{1/2}}[\hat{I}_{t|t}^{c1} - I_{t|t}^C - (\hat{I}_{t|t}^{c2} - I_{t|t}^C)] [\hat{I}_{t|t}^{c1} \\ &\quad - I_{t|t}^C - (\hat{I}_{t|t}^{c2} - I_{t|t}^C)]' \end{aligned} \quad (12)$$

and is equivalent to:

$$\mathbf{E}_{\mu_{1/2}}[\delta_t^C \delta_t^{C'}] = P_{I,t|t}^{c1} + P_{I,t|t}^{c2} - P_{I,t|t}^C - P_{I,t|t}^{C'} \quad (13)$$

The term $P_{I,t|t}^C$ denotes the associated covariance of fused current with its estimate $\hat{I}_{t|t}^C$. Also,

$$P_{I,t|t}^C = \mathbf{E}_{\mu_{1/2}}[(\hat{I}_{t|t}^{c1} - I_{t|t}^C)(\hat{I}_{t|t}^{c2} - I_{t|t}^C)'] = \mathbf{E}_{\mu_{1/2}}[\tilde{I}_{t|t}^{c1} \tilde{I}_{t|t}^{c2}] = P_{I,t|t}^{C'} \quad (14)$$

where $P_{I,t|t}^{C'}$ is the correlation between the two current estimates $\hat{I}_{t|t}^{c1}$ and $\hat{I}_{t|t}^{c2}$, respectively. Similarly, according to (10), $P_{I,t|t}^C$ can

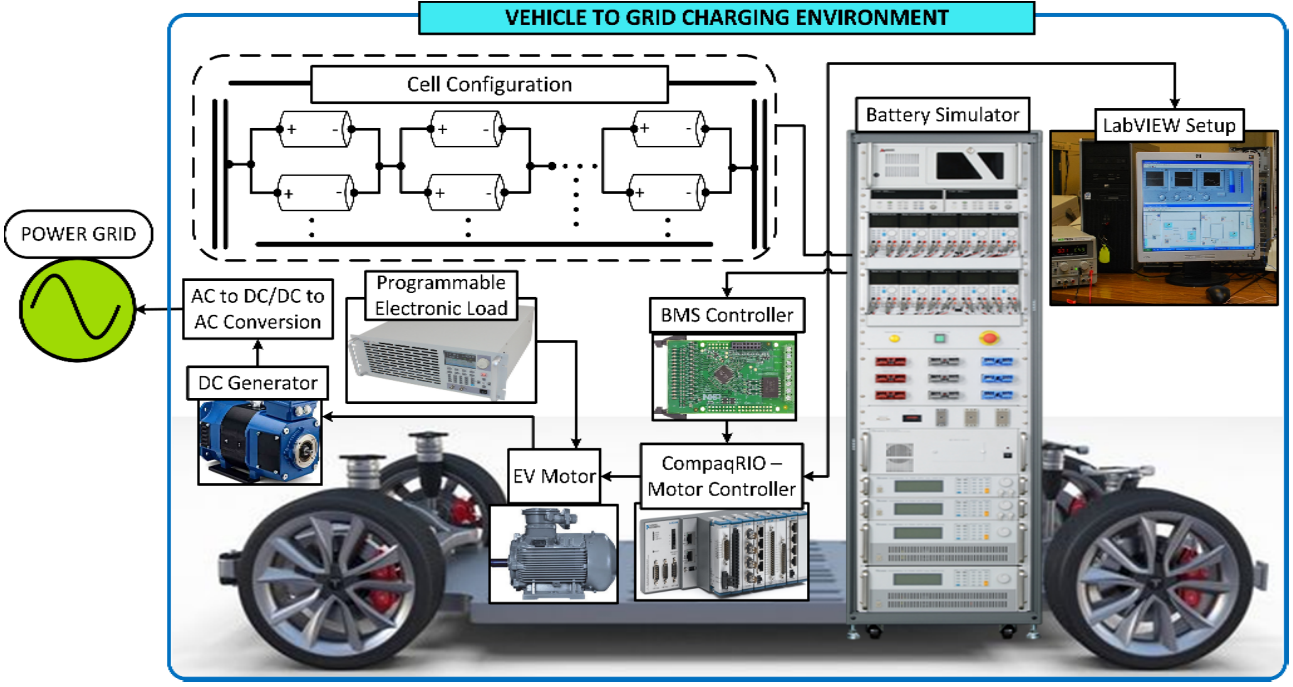


Fig. 4. Setup for V2G bi-directional charging system

be represented in the form of $P_{I,t|t}^{c1}$ and $P_{I,t|t}^{c2}$ as:

$$P_{I,t|t}^C = \frac{2P_{I,t|t}^{c1} P_{I,t|t}^{c2}}{F_t^C \alpha_t^C \beta_t^C (\omega \Xi_t^{c1} + (1-\omega) \Xi_t^{c2})} \quad (15)$$

where $\Xi_t^{c1} = P_{I,t|t}^{c1} \hat{I}_{t|t}^{c1} \Gamma_t^{c1} z_t^{c1}$ and $\Xi_t^{c2} = P_{I,t|t}^{c2} \hat{I}_{t|t}^{c2} \Gamma_t^{c2} z_t^{c2}$. However, there is a value for trace of split of current, which is dependent on variants of 1) change in temperature, 2) voltage fluctuation, and 3) external disturbances. Let the current at cell $c1$, I^{c1} consists of a correlated component I_{CR}^{c1} and an uncorrelated component I_{UC}^{c1} with respect to cell $c2$, such that $I^{c1} = I_{CR}^{c1} + I_{UC}^{c1}$, then the estimated covariance matrices for I_{CR}^{c1} and I_{UC}^{c1} will be $P_{I,CR,t}^{c1}$ and $P_{I,UC,t}^{c1}$ respectively. This gives a new definition of covariance matrices for cells $c1$ and $c2$ as:

$$P_{I,t|t}^{c1} = \frac{P_{I,CR,t|t}^{c1}}{\omega} + P_{I,UC,t}^{c1}, P_{I,t|t}^{c2} = \frac{P_{I,CR,t|t}^{c2}}{1-\omega} + P_{I,UC,t}^{c2} \quad (16)$$

Here ω can also be determined by optimizing an objective function in terms of ω , such that $\omega \in [0, 1]$. One of the possibilities of such an occurrence could be as the determinant of new covariance [31]. This gives the fused form of covariance matrices for cells $c1$ and $c2$. Representing in the form of correlated and uncorrelated current estimate measurements, it can be written as:

$$P_{I,CR,t|t}^C = P_{I,t|t}^C - P_{I,CR,t|t}^C \quad (17)$$

$$P_{I,UC,t|t}^C = P_{I,t|t}^C (P_{I,t|t}^{c1-1} P_{I,UC,t|t}^{c1} P_{I,t|t}^{c1-1} + P_{I,t|t}^{c2-1} P_{I,UC,t|t}^{c2} P_{I,t|t}^{c2-1}) P_{I,t|t}^C \quad (18)$$

Considering the correlated and uncorrelated measurements from cells $c1$ and $c2$ in (16), (10) becomes:

$$\hat{I}_{t|t}^C = P_{I,t|t}^C \left[\omega \left(\frac{\omega}{P_{I,CR,t|t}^{c1} + P_{I,UC,t|t}^{c1}} \right) \hat{I}_{t|t}^{c1} + (1-\omega) \left(\frac{1-\omega}{P_{I,CR,t|t}^{c2} + P_{I,UC,t|t}^{c2}} \right) \hat{I}_{t|t}^{c2} \right] \quad (19)$$

(19) can be further developed as:

$$\hat{I}_{t|t}^C = \left(\frac{\omega^2 F_t^C \hat{I}_{t|t}^{c1} P_{I,t|t}^{c1}}{P_{I,CR,t|t}^{c1} + P_{I,UC,t|t}^{c1}} \right) + \left(\frac{(1-\omega)^2 F_t^C \hat{I}_{t|t}^{c2} P_{I,t|t}^{c2}}{P_{I,CR,t|t}^{c2} + P_{I,UC,t|t}^{c2}} \right) \quad (20)$$

Taking the feedback for the update of current-split estimate gives,

$$P_{I,t|t}^{c-1} \hat{I}_{t|t}^C = -(N-1) P_{I,t|t}^{c-1} \hat{I}_{t|t}^C + \left(\frac{\omega^2 F_t^C \hat{I}_{t|t}^{c1} P_{I,t|t}^{c1}}{P_{I,CR,t|t}^{c1} + P_{I,UC,t|t}^{c1}} \right) + \left(\frac{(1-\omega)^2 F_t^C \hat{I}_{t|t}^{c2} P_{I,t|t}^{c2}}{P_{I,CR,t|t}^{c2} + P_{I,UC,t|t}^{c2}} \right) \quad (21)$$

where in-cell current variations can be iteratively updated at each time-instant t . $N = 2$ denotes the number of cells. The proof of convergence for covariance of in-cell current variations (20)-(21) are as follows.

Proof: This is proved in the Appendix. ■

Once the prediction of fused and in-cell variations have been calculated for estimation, a residual vector is generated to detect the variations.

5) *Step 5 - Determination of Residual Vector:* The residual of the estimated parameters is usually calculated to detect any 1) system-bias variation, and 2) sensor faults. These deviants could be detected for each measurement by (2). The representation for cells $c1$ and $c2$ can be made as:

$$y_t^{c1} = H_t^{c1} F_t^{c1} I_t^{c1} + \nu_t^{c1} \quad (22)$$

$$y_t^{c2} = H_t^{c2} F_t^{c2} I_t^{c2} + \nu_t^{c2} \quad (23)$$

Based on (22)-(23), a number of observations for N number of cells can be taken. Considering cell $c1$, the difference between the predicted output and the observations is calculated as:

$$\Upsilon_{t+1}^{c1} = [y_{t+1}^{c1} - \hat{y}_{t+1}^{c1}] = \sum_{i=1}^T \psi_{t-1}^i \theta_t^{c1(1)} \Delta I_t^{c1} + \nu_t^{c1} \quad (24)$$

where, the vector Υ_{t+1}^{c1} is the innovation calculated for cell $c1$. $\Delta I_t = I_t^f - I_t$ is the perturbation in I^{c1} . y_t^{c1} is the fault-free (nominal) output. y_t^{c1f} is the faulty output. $\theta_t^{c1(1)} = \frac{\delta \theta_t}{\delta I_t^{c1}}$, and ψ

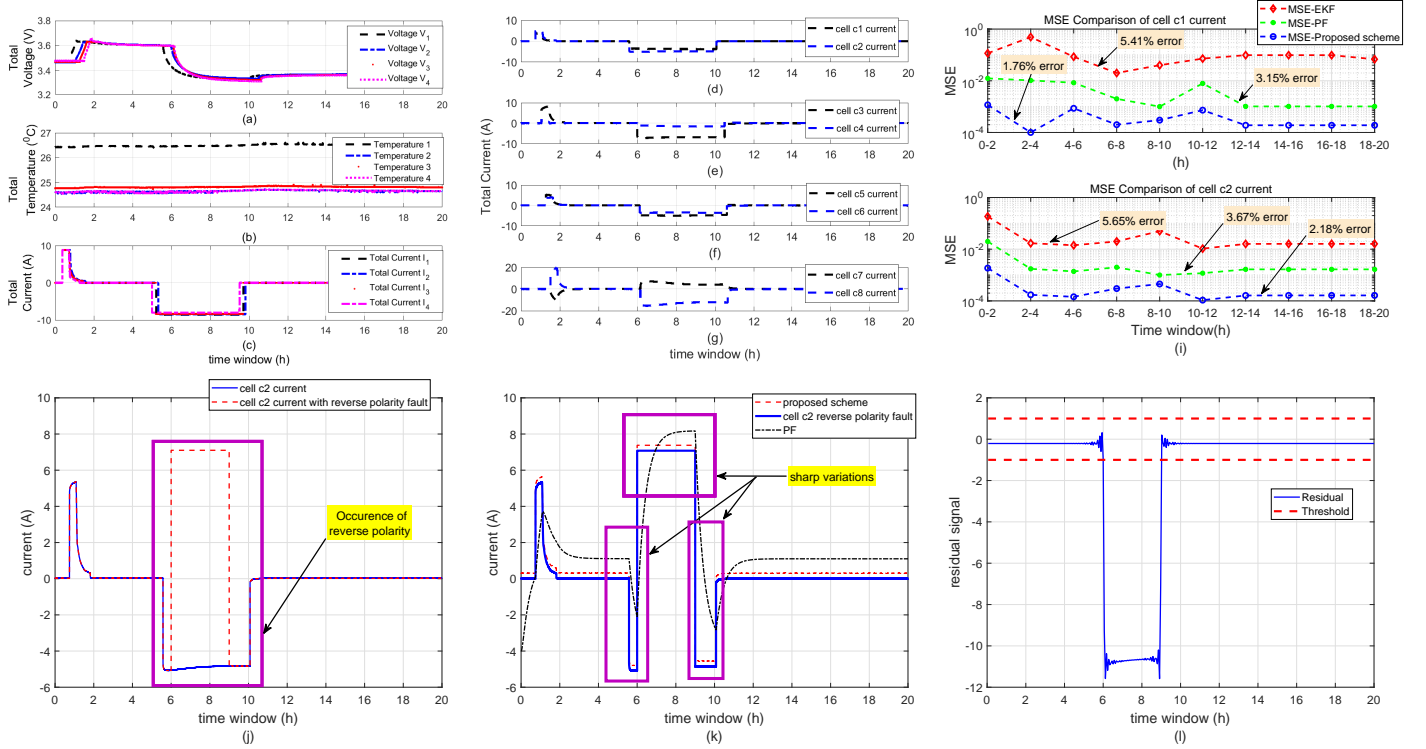


Fig. 5. Measurements of total a) voltage, b) temperature, and c) current. Measurements of current profile for cells d) c1, c2, e) c3, c4, f) c5, c6, g) c7 and c8 of Li-ion battery pack. MSE performance of current estimate in cells h) c1 and i) c2. Comparison of j) current profile in faulty cell c2, k) its estimate, and l) evaluation of residual signal

is the data vector formed of the past outputs and past reference inputs of cell $c1$. The gradient θ_t was estimated by performing a number of offline experiments for the cell $c1$. The input-output data from all the perturbed parameter experiments were then used to identify the gradients of cell $c1$, $\theta_t^{c1(1)}$. The outcome could be represented in the form of a density function between the faulty data and fault-free data. The variance S_{t+1} of this innovation can be found from (22) for cell $c1$ as:

$$\begin{aligned} S_{t+1}^{c1} &= \mathbf{E}_{\mu_{1/2}}(y_{t+1}^{c1} y_{t+1}^{c1'}) \\ &= F_t^{c1} P_{\mu_{1/2,t-1|t-1}}^{c1} F_t^{c1'} + \frac{\alpha_t^{c1}}{2} P_{\mu_{1/2,t-1|t-1}}^{var,\Gamma} \frac{\alpha_t^{c1'}}{2} \\ &\quad + \beta_t^{c1} P_{\mu_{1/2,t-1|t-1}}^{var,z} \beta_t^{c1'} + G_t^{c1} Q_t^{c1} G_t^{c1'} \end{aligned} \quad (25)$$

which shows the innovation covariance for cell $c1$.

Once the residuals vector $\mathcal{R}_{t+1}^{c1} = y_{t+1}^{c1} - \hat{y}_{t+1}^{c1}$ is yielded by comparing the estimation vector \hat{y}_t^{c1} with the measurements vector y_t , the fault isolation module is processed using the hypothesis model.

6) *Step 6 - Conditional Probability-based Hypothesis Model:* The conditional probability is developed using the hypothesis model M_t . The model represents the nominal (fault-free) operating mode of the cells at time $t+1$ given the expression for cell $c1$ as:

$$p_{I,t}(y_t^c) = \frac{g(y_{t+1}^c | M_t^{c1}, [y_t \dots y_T]) p_{I_t}(y_t^{c1})}{\sum_{j=0}^n (g(y_{t+1}^c | M_t^{c_j}, [y_t \dots y_T]) p_{I_t}(y_t^{c_j}))} \quad (26)$$

In (26), $g(\cdot)$ is the conditional probability density function of the measurement y_{t+1} , which is conditioned on the model M_t and the previous measurements. j is the number of corrupted cells from 0 to n . This function is determined by the expression

for cell $c1$ as:

$$g(y_{t+1}^c | M_t^{c1}, [y_t, \dots, y_T]) = \frac{e^{-\frac{1}{2} D_{t+1}^{c1}}}{(2\pi)^{\frac{m}{2}} |S_{t+1}^{c1}|^{\frac{1}{2}}} \quad (27)$$

D_{t+1} is the Mahalanobis distance at time $t+1$, which can be defined as the dissimilarity measure between the nominal (fault-free) and the faulty operating mode. m is the number of elements in the measurement vector.

The hypothesis model helps to process a validation gate for fault location.

7) *Step 7 - Validation Gate:* At each measurement collected from cells $c1$ and $c2$, a validation gate can be generated. It can be expressed for cell $c1$ as:

$$\mathcal{R}_{t+1}^{c1} S_{t+1}^{c1-1} \mathcal{R}_{t+1}^{c1'} = Q_t^{c1} \quad (28)$$

where (28) can be used to test observations for each cell in the circuit in order to determine the fault location.

III. IMPLEMENTATION AND EVALUATION

The proposed scheme was evaluated on a vehicle Li-ion battery-pack. The scheme was operated under different operating conditions. The experiments were conducted based on the guidelines issued by United States Department of Energy battery test manual [32,33]. The profiles of fault propagation were verified using D-SAT Chroma 8000ATS hardware platform. In order to evaluate the proposed methodology, a test case has been designed as shown in Fig. 4. The test case represents V2G bi-directional charging environment. The test case is dependent on the setup of floor combination of parallel cells, which are connected in a string of series. The online values of all the cells connected in this structure are plotted in Fig. 5, where Fig. 5 (a-

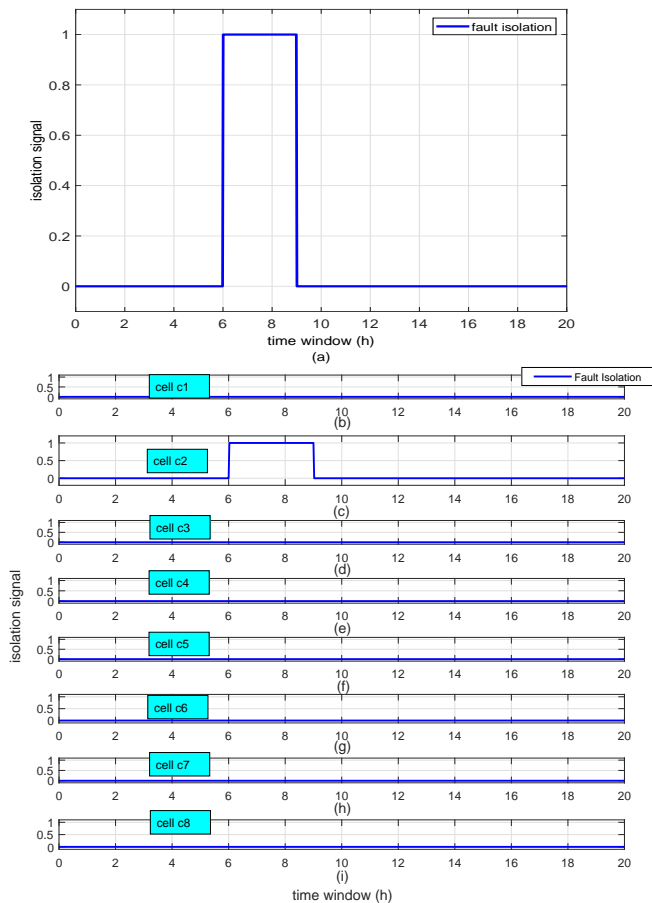


Fig. 6. Evaluation of fault a) isolation, and b-i) localization for injected reverse polarity fault in cell $c2$

c) shows the profiles of total voltage, total temperature and total current respectively. Fig. 5 (d-g) represents the current values of each cell in the floor. The test case considered a propagated reverse polarity fault in Fig. 1 with effect on cell $c2$. The proposed method is referenced with two mainstream techniques: 1) Extended Kalman filter (EKF) [34, 35], and 2) Particle filter (PF) [36]. The characterized battery cell considered has a nominal capacity of 2.3 Ah and a nominal voltage of 3.2 V. The experimental setup for verifying the fault propagation during bi-directional charging is composed of: 1) a D-SAT Chroma battery cell simulator with charging capacity of 2160 KWh, 2) an NXP BMS controller, 3) a DC motor, 4) a labVIEW-based compaqRIO controller for the motor, 5) a DC generator, 6) a boost DC-DC converter with a resonant circuit for a soft-switching and operation, 7) a programmable electronic load, 8) a data acquisition unit for collecting measurement signals, 9) data storage, and 10) a computer for controlling the current load and supply. The following tests were conducted with a frequency of 10 Hz at 20 °C: 1) characterization test, and 2) driving cycle test. The current is considered to be positive at discharge and negative at charge. Note the implementation was tested offline. This is because of two main reasons: 1) An injected fault can be detected by a BMS, which may result in compensation of the fault or system shutdown. 2) If the BMS is unable to detect the fault, the injected fault may result in potential damage to vehicle battery. These reasons may provide hinderance to the

proposed scheme while testing the whole set of considered fault situations. Therefore, the off-line approach has been chosen. Note the focus of this paper is to make an in-cell variation propagation analysis.

The purpose of this study is to examine the estimation and propagation analysis capability of the proposed scheme. A standard estimation analysis with no faults was made on the floor of cells $c1$ and $c2$. This was an initial analysis made to evaluate the performance of the proposed scheme towards estimating the regular cell dynamics without any injection. The current profiles of cells $c1$ and $c2$ were estimated. A comparison of mean square error (MSE) between the main stream EKF [34, 35], PF [36], and the proposed filter is shown in Fig. 5 (h)-(i). All the techniques performed reasonably well. However, the EKF started with a slow time tracking response, causing it to have a higher MSE value in the initial time windows. This is due to the lack of abrupt response in updating the covariance matrix at every iteration. This was due to the initialization procedure of EKF. This is not the case for PF. It performed better than EKF. However, the initial overshoot was not well-captured by the PF. This is due to its non-deterministic nature towards abrupt variations. In contrast, the proposed filter was fast enough to capture the dynamics well from the start.

Once a standard estimation analysis has been made, a test case was generated to evaluate the performance of the proposed filter in the presence of an injected fault. Cell $c2$ suffered from a reverse polarity fault in the middle of the charging cycle from 6.0–9.0 h as shown in Fig. 5 (j). This could be possibly due to an operational fault in BMS caused by a shorted diode inside the cell. This may also reverse the electro-mechanical process and an acceleration in current flow, resulting in high electrical leakage among the cells and the circuit. This could possibly lead to burnout due to a thermal run-away chain reaction and a shorted capacitor [37]. A comparison of estimates between the main stream PF [36] and the proposed scheme can be seen in Fig. 5 (k). The proposed method gives more accurate results than PF. It also managed to estimate the deviations of the profile with precision. This is due to its predictive nature using the innovation process used for the initialization. Furthermore, fault detection has been made by generating a residual vector to calculate variations between the fault-free and faulty profile of the cell $c2$. The threshold selected for current was ± 1 . Referring to Fig.5 (l), the fault was detected using the threshold selection. Fault isolation and localization can be observed in Fig. 6 (a) and Fig. 6 (g-i) respectively. By applying conditional probability-based hypothesis model and validation gate, the operator can clearly analyze the fault occurrence in cell $c2$.

The faulty cell $c2$ also made a propagation impact on other parameters of the circuit as follows:

- *First Propagation:* A step-like rise in voltage $V_{2,t}$ is noticed from 6.0 to 9.1 h.
- *Second Propagation:* A spike variation in temperature $\Gamma_{2,t}$ is seen from 13.6 to 15.5 h respectively.
- *Third Propagation:* A step-like variation is observed in voltage $V_{4,t}$ from 6.0 to 9.2 h respectively.

The first propagation illustrates a step-like variation of voltage $V_{2,t}$ collected from the floor of cells $c1$ and $c2$. The second propagation represents a rise in temperature $\Gamma_{4,t}$. This is the

impact of resilience shown by the impedance of cells $c7$ and $c8$ towards the faulty cell $c2$. The third propagation imitates a similar fluctuation pattern in voltage $V_{4,t}$ like the propagated $V_{2,t}$. This is the reaction of temperature $T_{2,t}$ and the floor of cells $c5$ and $c6$. All the propagations can be seen in Fig.7 (a)-(c).

First Propagation: The variation propagation of the reverse polarity in cell $c2$ was estimated. The first propagation consisted of a large variations across 8.0–14.2 h monitoring window. As a result, the estimation accuracy is impacted. While the window of 8.0–14.2 h could represent the impact of fault propagation, an effect due to the dynamic variations can be seen in a window of 1.0–1.5 h. However, the proposed method was able to estimate the variations with adequate precision. The PF [36] was slow in estimating the sharp variations as shown in Fig. 7 (d). The reverse polarity fault was detected and isolated appropriately as shown in Fig.7 (e)-(f). The threshold selected for residual was ± 1 .

Second Propagation: In the second propagation, the temperature sensor generated a large number of wiggles affecting window 16.2–19.8 h. Due to the high magnitude of variations, a semi-logarithmic plot was selected to monitor the estimation accuracy. The proposed scheme still computed accurate estimations. On the other hand, PF failed to capture the wiggles. This might be due to the congregation of sample measurements while predicting instant variations. The estimation comparison can be seen in Fig. 7 (g). Fault detection and isolation was proposed by using an interval-based adaptive threshold. As observed, the high variations in temperature are observed only in the positive values of temperature. Therefore, the threshold was active only in the positive scale. The evaluation can be seen in Fig.7 (h)-(i).

Third Propagation: Next, the third propagation was examined. Since, the propagation contained amplitudes and characteristics similar to first propagation, a semi-logarithmic plot was considered to monitor the variations as shown in Fig. 7 (j). The main stream PF lost the track assuming the independence of the observations without gaining any new information. The threshold selection algorithm was adequate to detect the variations by selecting a threshold of ± 2 while avoiding any false alarms. Subsequently, accurate detection signal was generated for fault isolation. The evaluation can be followed in Fig.7 (k)-(l).

IV. CONCLUSIONS

In this paper, an in-cell variation and propagation of a vehicle battery involved in V2G technologies has been analyzed. This is achieved by median expectation-based prediction approach to estimate the in-cell variations and split of current in the floor of arrays of cells. To enhance the analysis of these variations at the local level, the prediction structure is supported by the residual vector and hypothesis model. The proposed scheme has been demonstrated to improve the service life of the battery pack in EV, and thereby boost the effectiveness of power grid ancillary services. Estimation comparison of the scheme was made with two existing mainstream techniques of automotive lithium-ion batteries, extended Kalman filter and particle filter. In the future, studies will be conducted to quantitatively analyze the vehicular technology operations while considering the developed in-cell variations as an exogenous variable.

APPENDIX

Proof of Convergence for (20) and (21): Since the current-split estimates of cell $c1$ and $c2$ are defined in (16), the estimation shall be converging if:

$$P_{I,C\mathcal{R},t|t}^{c1} \geq \mathbf{E}_{\mu_{1/2}} [(I_{C\mathcal{R},t|t}^{c1} - \hat{I}_{C\mathcal{R},t|t}^{c1})(I_{C\mathcal{R},t|t}^{c1} - \hat{I}_{C\mathcal{R},t|t}^{c1})'] \quad (29)$$

$$P_{I,UC,t|t}^{c1} \geq \mathbf{E}_{\mu_{1/2}} [(I_{UC,t|t}^{c1} - \hat{I}_{UC,t|t}^{c1})(I_{UC,t|t}^{c1} - \hat{I}_{UC,t|t}^{c1})'] \quad (30)$$

$$P_{I,C\mathcal{R},t|t}^{c2} \geq \mathbf{E}_{\mu_{1/2}} [(I_{C\mathcal{R},t|t}^{c2} - \hat{I}_{C\mathcal{R},t|t}^{c2})(I_{C\mathcal{R},t|t}^{c2} - \hat{I}_{C\mathcal{R},t|t}^{c2})'] \quad (31)$$

$$P_{I,UC,t|t}^{c2} \geq \mathbf{E}_{\mu_{1/2}} [(I_{UC,t|t}^{c2} - \hat{I}_{UC,t|t}^{c2})(I_{UC,t|t}^{c2} - \hat{I}_{UC,t|t}^{c2})'] \quad (32)$$

Considering (18), the difference between the fused uncorrelated covariance for cells $c1$, $c2$ and $\mathbf{E}[(I_{UC,t|t}^C - \hat{I}_{UC,t|t}^C)(I_{UC,t|t}^C - \hat{I}_{UC,t|t}^C)']$:

$$\begin{aligned} &= P_{I,t|t}^C (P_{I,t|t}^{c1-1} P_{I,UC,t|t}^{c1} P_{I,t|t}^{c1-1} + P_{I,t|t}^{c2-1} P_{I,UC,t|t}^{c2} P_{I,t|t}^{c2-1}) P_{I,t|t}^C \\ &- P_{I,t|t}^C (P_{I,t|t}^{c1-1} \mathbf{E}_{\mu_{1/2}} [(I_{UC,t|t}^{c1} - \hat{I}_{UC,t|t}^{c1})(I_{UC,t|t}^{c1} - \hat{I}_{UC,t|t}^{c1})'] P_{I,t|t}^{c1-1} \\ &+ P_{I,t|t}^{c2-1} \mathbf{E}_{\mu_{1/2}} [(I_{UC,t|t}^{c2} - \hat{I}_{UC,t|t}^{c2})(I_{UC,t|t}^{c2} - \hat{I}_{UC,t|t}^{c2})'] P_{I,t|t}^{c2-1}) P_{I,t|t}^C \\ &= P_{I,t|t}^C (P_{I,t|t}^{c1-1} (P_{I,UC,t|t}^{c1-1} - \mathbf{E}_{\mu_{1/2}} [(I_{UC,t|t}^{c1} - \hat{I}_{UC,t|t}^{c1})(I_{UC,t|t}^{c1} \\ &- \hat{I}_{UC,t|t}^{c1})'] P_{I,t|t}^{c1-1} + P_{I,t|t}^{c2-1} (P_{I,UC,t|t}^{c2-1} - \mathbf{E}_{\mu_{1/2}} [(I_{UC,t|t}^{c2} - \hat{I}_{UC,t|t}^{c2}) \\ &(I_{UC,t|t}^{c2} - \hat{I}_{UC,t|t}^{c2})'] P_{I,t|t}^{c2-1}) P_{I,t|t}^C \geq 0 \quad (33) \end{aligned}$$

Similarly, considering (16) for correlated covariance, the convergence for the $P_{I,C,t|t}^C - \mathbf{E}_{\mu_{1/2}} [(I_{C,t|t}^C - \hat{I}_{C,t|t}^C)(I_{C,t|t}^C - \hat{I}_{C,t|t}^C)']$ can be achieved.

ACKNOWLEDGMENTS

The authors thank Associate Research Professor Qadeer Ahmed from Center for Automotive Research, The Ohio State University for his insights and suggestions.

REFERENCES

- [1] R. A. Raustad, "The role of V2G in the smart grid of the future," *Interface*, vol. 24, no. 1, pp. 53–60, 2015.
- [2] S. Morse and K. Glitman, "Electric vehicles as grid resources in ISO-NE and Vermont," <https://www.veic.org/documents/default-source/resources/reports/evt-rd-electric-vehicles-grid-resource-final-report.pdf>, *Tech. Report*, pp. 1–44, May 2014.
- [3] H. Xing, Z. Lin, M. Fu, "A new decentralized algorithm for optimal load shifting via electric vehicles," *Proc. 36th Chinese Ctrl. Conf.*, Dalian, China, pp. 10708–10713, July 26–28, 2017.
- [4] G. Wenzel, M. Negrete-Pincetic, D. E. Olivares, J. MacDonald, and D. S. Callaway, "Real-time charging strategies for an electric vehicle aggregator to provide ancillary services," *IEEE Trans. Smart Grid*, vol. 9, no. 5, pp. 5141–5151, Article in Press, 2018.
- [5] X. Wang, and Q. Liang, "Energy management strategy for Plug-In hybrid electric vehicles via bidirectional Vehicle-to-Grid," *IEEE Systems J.*, vol. 11, no. 3, pp. 1789–1798, Sep. 2017.
- [6] R. Sioshansi and P. Denholm, "The value of plug-in hybrid electric vehicles as grid resources," *The Energy J.*, vol. 31, no. 3, pp. 1–23, 2010.
- [7] R. Loisel, G. Pasaoglu, and C. Thiel, "Large-scale deployment of electric vehicles in Germany by 2030: An analysis of grid-to-vehicle and vehicle-to-grid concepts," *Energy Policy*, vol. 65, pp. 432–443, 2014.
- [8] C. D. Whitea, K. M. Zhang, "Using vehicle-to-grid technology for frequency regulation and peak-load reduction," *J. Pow. Sources*, vol. 196, no. 8, pp. 3972–3980, 2011.
- [9] S. Das, K. M. Salim, D. Chowdhury, "A novel variable width PWM switching based buck converter to control power factor correction phenomenon for an efficacious grid integrated electric vehicle battery charger," *TENCON, IEEE Region 10 Conf.*, Malaysia, pp. 262–267, 5–8 Nov. 2017.
- [10] S. Das, K. M. Salim, D. Chowdhury, M. M. Hasan, "Inverse sinusoidal pulse width modulation switched electric vehicles' battery charger," *Intl. J. Elec. Comp. Engg.*, vol. 9, no. 5, pp. 3344–3358, Oct. 2019.

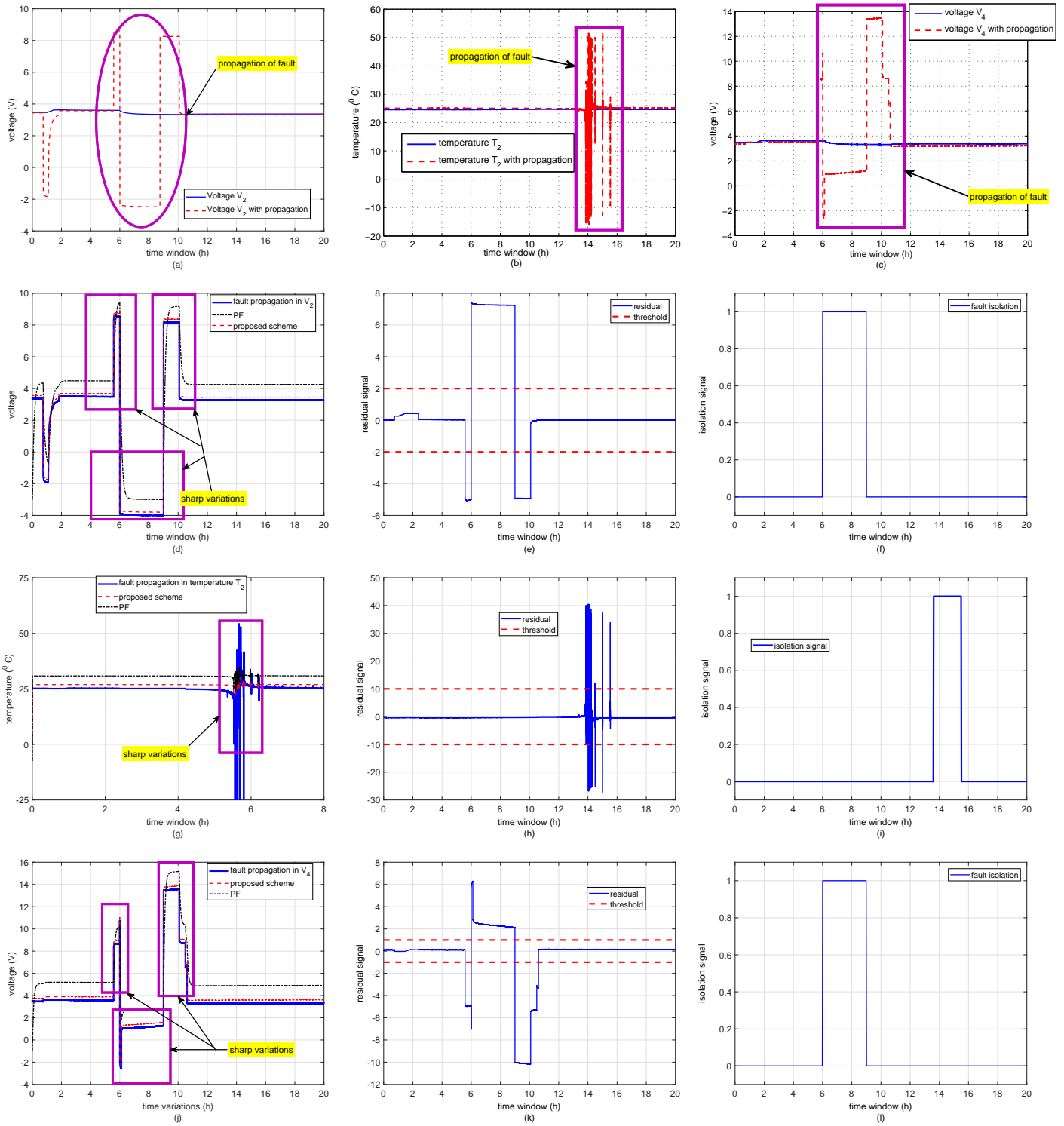


Fig. 7. Propagation of injected reverse polarity fault on cell c_2 with its impact on a) voltage $V_{2,t}$, b) temperature $T_{2,t}$, and c) voltage $V_{4,t}$, Comparison of estimate for fault propagation and its evaluation of residual signal and fault isolation in d-f) voltage $V_{2,t}$, g-i) temperature $T_{2,t}$, j-l) voltage $V_{4,t}$, respectively

- [11] L. Su, J. Zhang, C. Wang, Y. Zhang, Z. Li, Y. Song, T. Jin, and Z. Ma, "Identifying main factors of capacity fading in lithium ion cells using orthogonal design of experiments," *Applied Energy*, vol. 163, pp. 201–210, Feb. 2016.
- [12] S. J. Harris, D. J. Harris, and C. Li, "Failure statistics for commercial lithium ion batteries: A study of 24 pouch cells," *J. Power Sources*, vol. 342, pp. 589–597, Feb. 2017.
- [13] D. P. Abraham, E. P. Roth, R. Kosteccki, K. McCarthy, S. MacLaren, S., and D. H. Doughty, "Diagnostic examination of thermally abused high-power Li-ion cells," *J. Power Sources*, vol. 161, no. 1, pp. 648–657, Oct. 2006.
- [14] Q. S. Wang, P. Ping, X. J. Zhao, G. Q. Chu, J. H. Sun, and C. H. Chen, "Thermal runaway caused fire and explosion of Li-ion battery," *J. Power Sources*, vol. 208, pp. 210–224, Jun. 2012.
- [15] C. Mikolajczak, M. Kahn, K. White, K., and R. T. Long, R.T. "Li-ion batteries hazard and use assessment," *Fire Protection Research Foundation - Final Report*, pp. 1–126, Jul. 2011.
- [16] H. D. Daniel, and A. P. Ahmad, "Vehicle battery safety roadmap guid-

- ance,” *Battery Safety Consulting (subcontractor), NREL Report No. SR-5400-54404*, pp. 1–131, Oct. 2012.
- [17] R. Xiong, Y. Zhang, J. Wang, H. He, S. Peng, and M. Pecht, “Lithium-ion battery health prognosis based on a real battery management system used in electric vehicles,” *IEEE Trans. Vehicular Tech.*, pp. 1–10, Article in Press, 2018.
- [18] B. G. Carkhuff, P. A. Demirev, and R. Srinivasan, “Impedance-based battery management system for safety monitoring of Lithium-Ion batteries,” *IEEE Trans. Industrial Electronics*, vol. 65, no. 8, pp. 6497–6504, 2018.
- [19] D. F. Frost, and D. A. Howey, “Completely decentralized active balancing battery management system,” *IEEE Trans. Power Electronics*, vol. 33, no. 1, pp. 729–738, 2018.
- [20] H. M. Khalid, Q. Ahmed and J. C.-H. Peng, “Health Monitoring of Li-ion battery systems: A median expectation-based diagnosis approach (MEDA),” *IEEE Trans. Transp. Elec.*, vol. 1, no. 1, pp. 94–105, Jul. 2015.
- [21] D. Andre, C. Appel, T. Soczka-Guth, D. U. Sauer, “Advanced mathematical methods of SOC and SOH estimation for lithium-ion batteries,” *J. Power Sources*, vol. 224, pp. 2027, Feb. 2013.
- [22] Y. He, X. Liu, C. Zhang, Z. Chen, “A new model for State-of-Charge (SOC) estimation for high-power Li-ion batteries,” *Applied Energy*, vol. 101, pp. 808–814, Jan. 2013.
- [23] A. Marongiu, M. Roscher, D. U. Sauer, “Influence of the vehicle-to-grid strategy on the aging behavior of lithium battery electric vehicles,” *Applied Energy*, vol. 137, pp. 899–912, Jan. 2015.
- [24] M. Dubarry, A. Devie and M. Katherine, “Durability and reliability of electric vehicle batteries under electric utility grid operations: Bidirectional charging impact analysis,” *J. Power Sources*, vol. 358, pp. 39–49, Aug. 2017.
- [25] G. Rancilio, “Battery energy storage systems for ancillary services provision,” *Thesis*, Department of Energy, Politecnico Di Milano, pp. 1–154, 2018.
- [26] M. S. Grewal, V. Henderson, V., and R. Miyasako, R., “Application of Kalman filtering to the calibration and alignment of inertial navigation systems,” *IEEE Trans. Automatic Ctrl.*, vol. 36, no. 1, pp. 4–14, Jan. 1991.
- [27] H. Hijazi, and L. Ros, “Joint data QR-detection and Kalman estimation for OFDM time-varying Rayleigh channel complex gains,” *IEEE Trans. Communications*, vol. 58, no. 1, pp. 170–178, Jan. 2010.
- [28] G. Kurz, I. Gilitschenski, and U. D. Hanebeck, “Recursive Bayesian filtering in circular state spaces,” *IEEE Aerospace and Electronic Systems Magazine*, vol. 31, no. 3, pp. 70–87, 2016.
- [29] A. C.-Arenas, S. Onori, G. Rizzoni, “A control-oriented lithium-ion battery pack model for plug-in hybrid electric vehicle cycle-life studies and system design with consideration of health management,” *J. Power Sources*, vol. 279, pp. 791–808, Apr. 2015.
- [30] N. J. Gordon, D. J. Salmond, and A. F. M. Smith, “Novel approach to non-linear/non-Gaussian Bayesian state estimation,” *IEEE Proceedings*, vol. 140, no. 2, pp. 107–113, 1993.
- [31] S. J. Julier, and J. K. Uhlmann, “General decentralized data fusion with covariance intersection (CI),” in *Hdbook. Data Fus.*, D. Hall and J. Linas, Eds. Boca Raton, FL, USA: CRC Press, 2001, ch. 12.
- [32] J. Marcicki, M. Canova, M., A. T. Conlisk, and G. Rizzoni, “Design and parametrization analysis of a reduced-order electrochemical model of graphite/ $LiFePO_4$ cells for SOC/SOH estimation,” *J. Power Sources*, vol. 237, pp. 310–324, Sep. 2013.
- [33] “Battery test manual for Plug-In hybrid electric vehicles,” *U.S. Dept. Ener. Vehicle Tech. Program*, Mar. 2008.
- [34] A. Singh, A. Izadian, and S. Anwar, “Adaptive nonlinear model-based fault diagnosis of Li-ion Batteries,” *IEEE Trans. Indus. Elect.*, vol. 62, no. 2, pp. 1002–1011, Jul. 2014.
- [35] H. He, R. Xiong, X. Zhang, F. Sun, and J. Fan, “State-of-Charge estimation of the lithium-ion battery using an adaptive extended Kalman filter based on an improved Thevenin model,” *IEEE Trans. Vehicular Tech.*, vol. 60, no. 4, pp. 1461–1469, May 2011.
- [36] S. Schwunk, N. Armbruster, S. Straub, J. Kehl, M. Vetter, “Particle filter for state of charge and state of health estimation for lithiumiron phosphate batteries,” *J. Power Sources*, vol. 239, pp. 705–10, Oct. 2013.
- [37] “Protecting vehicle electronics from reverse battery connection,” *link: <https://www.diodes.com/design/suport/technical-articles/protecting-vehicle-electronics-from-reverse-battery-connection/>*, 2017.

Biography



Haris M. Khalid (M'13) received his B.S. (Hons.) degree in Mechatronics and Control Systems Engineering from University of Engineering and Technology (UET), Lahore, Pakistan, in 2007, and the M.S. and Ph.D. degrees in Control Systems Engineering from King Fahd University of Petroleum and Minerals (KFUPM), Dhahran, KSA, in 2009 and 2012, respectively. He is currently an Assistant Professor in Electrical and Electronics Engineering with the Higher Colleges of Technology (HCT), Sharjah Campuses, UAE. In 2012, he joined Distributed Control Research Group (DCRG) at KFUPM, as a Research Fellow. From 2013 to 2016, he worked as a Research Fellow with the Power Systems

Research Laboratory (PSRL) at iCenter for Energy, Masdar Institute (MI), Khalifa University of Science and Technology, Abu Dhabi, UAE, which is an MI-MIT Cooperative Program with Massachusetts Institute of Technology (MIT), Cambridge, MA, USA. During this tenure, he also worked as a Visiting Scholar at Energy Systems, Control & Optimization Lab at ADNOC Research & Innovation Center, Khalifa University of Science and Technology, Abu Dhabi, UAE. He has authored/co-authored over 60 peer-reviewed research publications. He has served as an Energy Specialist in UAE Space Agency (UAESA) 'Tests in Orbit' Competitions, which are partnered with Dream-up and Nano-Racks. He has also served as the Technical Chair of IEEE-ASET'2018-2020 (Seven Group of Conferences) organized in UAE. He is also a reviewer to IEEE Transactions on Power Systems, Neural Network and Learning Systems, Control of Network Systems, Transportation Electrification, and IEEE Systems Journal. His current research interests include power systems, cyber-physical systems, electric vehicles, signal processing, V2G Technology, fault diagnostics, filtering, estimation, and condition monitoring.



Jimmy C.-H. Peng (S'04-M'12) received the B.E. and Ph.D. degrees in electrical and computer engineering from the University of Auckland, Auckland, New Zealand, in 2008 and 2012, respectively. He is currently an Assistant Professor in electrical and computer engineering with the National University of Singapore, Singapore. Previously, he was an Assistant Professor with the Masdar Institute (now part of the Khalifa University), Abu Dhabi, United Arab Emirates. In 2013, he was appointed a Visiting Scientist with the Research Laboratory of Electronics, Massachusetts Institute

of Technology, Cambridge, MA, USA, where he became a Visiting Assistant Professor in 2014. His research interests include power system stability, cyber security, microgrids, and high-performance computing. He is currently the Secretary of the IEEE Power and Energy Society Working Group on High-Performance Computing for Power Grid Analysis and Operation. He is also a Committee Member for Singapore Standard SS 535.